Journal of Experimental Botany, Vol. 68, No. 2 pp. 299–310, 2017
doi:10.1093/jxb/erw357 Advance Access publication 4 October 2016
This paper is available online free of all access charges (see http://jxb.oxfordjournals.org/open_access.html for further details)

RESEARCH PAPER

Effects of reduced carbonic anhydrase activity on CO_2 assimilation rates in *Setaria viridis*: a transgenic analysis

Hannah L. Osborn[1], Hugo Alonso-Cantabrana[1,*], Robert E. Sharwood[1], Sarah Covshoff[2], John R. Evans[1], Robert T. Furbank[1] and Susanne von Caemmerer[1]

[1] Australian Research Council Centre of Excellence for Translational Photosynthesis, Division of Plant Sciences, Research School of Biology, The Australian National University, Acton, ACT 2601, Australia
[2] Department of Plant Sciences, University of Cambridge, Cambridge CB2 3EA, UK

* Correspondence: Hugo.Alonso@anu.edu.au

Received 19 July 2016; Accepted 5 September 2016

Editor: Christine Raines, University of Essex

Abstract

In C_4 species, the major β-carbonic anhydrase (β-CA) localized in the mesophyll cytosol catalyses the hydration of CO_2 to HCO_3^-, which phospho*enol*pyruvate carboxylase uses in the first step of C_4 photosynthesis. To address the role of CA in C_4 photosynthesis, we generated transgenic *Setaria viridis* depleted in β-CA. Independent lines were identified with as little as 13% of wild-type CA. No photosynthetic defect was observed in the transformed lines at ambient CO_2 partial pressure (pCO_2). At low pCO_2, a strong correlation between CO_2 assimilation rates and CA hydration rates was observed. $C^{18}O^{16}O$ isotope discrimination was used to estimate the mesophyll conductance to CO_2 diffusion from the intercellular air space to the mesophyll cytosol (g_m) in control plants, which allowed us to calculate CA activities in the mesophyll cytosol (C_m). This revealed a strong relationship between the initial slope of the response of the CO_2 assimilation rate to cytosolic pCO_2 (AC_m) and cytosolic CA activity. However, the relationship between the initial slope of the response of CO_2 assimilation to intercellular pCO_2 (AC_i) and cytosolic CA activity was curvilinear. This indicated that in *S. viridis*, mesophyll conductance may be a contributing limiting factor alongside CA activity to CO_2 assimilation rates at low pCO_2.

Key words: Carbonic anhydrase, $C^{18}O^{16}O$ isotope discrimination, C_4 photosynthesis, mesophyll conductance, *Setaria viridis*, transformation

Introduction

C_4 plants have evolved a CO_2-concentrating mechanism (CCM) that enables the elevation of CO_2 around the active sites of Rubisco by a combination of anatomical and biochemical specialization (Hatch, 1987). C_4 photosynthesis has independently evolved >60 times, providing one of the most widespread and effective solutions for remedying the catalytic inefficiency of Rubisco (Sage *et al.*, 2012; Christin and Osborne, 2013). The key carboxylases in C_4 plants are localized to different cellular compartments. Phospho*enol*pyruvate carboxylase (PEPC) is localized to the cytosol of mesophyll cells and Rubisco to the chloroplasts of bundle sheath cells. For the CCM to operate effectively, PEPC activity must exceed Rubisco activity to balance leakage of CO_2 out of the bundle sheath compartment. This maintains a high bundle sheath CO_2 level but prevents wasteful overcycling of the mesophyll CO_2 'pump' (von Caemmerer and Furbank, 2003). As PEPC utilizes HCO_3^- and not CO_2, the first committed enzyme of the C_4 pathway is carbonic anhydrase (CA) which

catalyses the reversible conversion of CO_2 and HCO_3^- in the cytosol of mesophyll cells. C_4 acids produced by PEPC then diffuse into the bundle sheath cells where they are decarboxylated, supplying CO_2 for Rubisco.

Within higher plants, there are multiple forms of the α-CA, β-CA, and γ-CA families which share little sequence homology (Moroney *et al.*, 2001). β-CAs are the most prevalent CA family in land plants. CA is an abundant enzyme in C_3 plants, representing up to 2% of the soluble leaf protein (Okabe *et al.*, 1984). In C_3 plants, the role of CA is unclear (Badger and Price, 1994) as it does not appear to limit photosynthesis but does influence stomatal conductance, guard cell movement, and amino acid biosynthesis (Hu *et al.*, 2010; DiMario *et al.*, 2016; Engineer *et al.*, 2016).

It has long been contended that the uncatalysed rate of CO_2 conversion to HCO_3^- is insufficient to support C_4 photosynthetic flux (Hatch and Burnell, 1990; Badger and Price, 1994). This hypothesis was supported by experiments in the C_4 dicot *Flaveria bidentis*, where antisense plants with <10% of wild-type CA activity required high CO_2 for growth and showed reduced CO_2 assimilation rates (von Caemmerer *et al.*, 2004; Cousins *et al.*, 2006). However, in the C_4 monocot *Zea mays* mutant plants with reduced CA activity (3% of wild type), no limitation to CO_2 assimilation rates at ambient CO_2 was observed (Studer *et al.*, 2014). CA activity has been shown to vary widely between species (Cousins *et al.*, 2008), and it is unclear whether CA activities are limiting at high CO_2 assimilation rates, as has previously been suggested (Hatch and Burnell, 1990; Gillon and Yakir, 2000).

We examined the role of CA in the model C_4 monocot species *Setaria viridis* (green foxtail millet). *Setaria viridis* is closely related to agronomically important C_4 crops including *Z. mays* (maize), *Sorghum bicolor* (sorghum), and *Saccharum officinarum* (sugarcane) (Brutnell *et al.*, 2010). It is an ideal model species due to its rapid generation time, small stature, high seed production, diploid status, and small genome that is sequenced and publicly available (Doust *et al.*, 2009; Brutnell *et al.*, 2010; Li and Brutnell, 2011). Here we used a stable transformation approach to examine the role of CA in *S. viridis* and could show that *S. viridis* is a useful model species that lends itself to molecular manipulation of the C_4 photosynthetic pathway. Two constructs both targeting the major leaf β-CA (Si003882m.g) were used to generate three independent transformed lines with reduced CA activity. A strong correlation between the CO_2 assimilation rate at low pCO_2 and CA activity was observed. Our combined measurements of mesophyll conductance and CA activity suggest that increasing mesophyll conductance may be an important way to increase the CO_2 assimilation rate at low intercellular pCO_2, as may occur under drought.

Materials and methods

Plant growth conditions

T_1 seeds were incubated in 5% liquid smoke (Wrights) for 24 h to promote germination, and germinated in garden soil mix fertilized with Osmocote (Scotts, Australia) in small containers before being transferred to individual 2 litre pots. Plants were grown in controlled environmental chambers, irradiance 500 µmol photons m^{-2} s^{-1}, 16 h photoperiod, 28 °C day, 24 °C night, 2% CO_2. Pots were watered daily.

Construct generation

Two different constructs were used to generate three lines of reduced CA activity. First, an RNAi was targeted to the primary leaf β-CA Si003882m which generated lines 2.1 and 5.3. A region of Si003882m.g was amplified by PCR using gene-specific primers (Supplementary Table S1 at *JXB* online) and reverse-transcribed RNA from *S. viridis* leaves ligated into pENTR/D-TOPO (ThermoFisher), and verified by sequencing. The fragment was inserted via a double Gateway system LR reaction (Invitrogen) into the hairpin RNAi binary vector pSTARGATE (Greenup *et al.*, 2010) to form a stem–loop region under the control of the ubiquitin promoter/intron (UBI) and octopine synthase (OCS) terminator to form the RNAi vector pSG/*CAa*.

Secondly, an overexpression approach, which resulted in gene silencing, generated the third transformed line, 1.1. The coding sequence of the maize β-CA gene (GRMZM2G348512), *ZmCA2* (Studer *et al.*, 2014), was amplified by reverse transcription–PCR (RT–PCR) from total RNA extracted from B73 maize. Total RNA was isolated using hot acid phenol and chloroform, and then treated with RQ1 RNase-free DNase (Promega). The reverse transcription and PCRs were performed as per the manufacturer's protocols with Superscript II (ThermoFisher) and Phusion High-Fidelity DNA polymerase (NEB), respectively (for primers, see Supplementary Table S1). The sequence encoding an AcV5 epitope tag (Lawrence *et al.*, 2003) was added to the C-terminal end of *ZmCA2*. The resulting *ZmCA2* amplicon was cloned into pENTR/D-TOPO and verified by sequencing. LR Gateway cloning (ThermoFisher) was used to insert the *ZmCA2* coding sequence into the overexpression vector, pSC110. pSC110 was created by Gibson Assembly (Gibson *et al.*, 2009) from two modified pMDC164 vectors (Curtis and Grossniklaus, 2003), kindly provided to us by Udo Gowik (Heinrich-Heine University, Dusseldorf, Germany). *ZmCA2* expression from pSC110 was driven by the B73 *ZmPEPC* promoter. pSC110 and pSC110/*ZmCA2* were verified by sequencing.

Both constructs were transformed into *Agrobacterium tumefaciens* strain AGL1 for stable plant transformation.

Callus induction and plant transformation

Stable transformation of *S. viridis* (accession A10.1) was carried out as described by Brutnell *et al.* (2010). Seed coats were mechanically removed from mature *S. viridis* seeds to improve germination. Seeds were sterilized before plating on callus induction medium [CIM; 4.3 g l^{-1} Murashige and Skoog (MS) salts, pH 5.8, 10 ml l^{-1} 100× MS vitamins stock, 40 g l^{-1} maltose, 35 mg l^{-1} $ZnSO_4 \cdot 7H_2O$, 0.6 mg l^{-1} $CuSO_4 \cdot 5H_2O$, 4 g l^{-1} Gelzan, 0.5 mg l^{-1} kinetin, 2 mg l^{-1} 2,4-D]. After 4 weeks in the dark at 24 °C, any seedling structures or gelatinous calli were removed and remaining calli transferred to fresh CIM. After a further 2 weeks, calli were divided and replated onto fresh CIM. One week later, transformations were performed.

AGL1 containing the construct of interest were grown in the presence of 50 µg l^{-1} kanamycin and 50 µg l^{-1} rifampicin at 28 °C to OD_{600}=0.5 and then resuspended in CIM without Gelzan and hormones. Acetosyringone (200 mM) and synperonic [0.01% (w/v)] were added to the *Agrobacterium* solution before incubating the calli in the medium for 5 min at room temperature. The calli were blotted dry on sterile filter paper and incubated at 22 °C for 3 d in the dark. The calli were then transferred to selective CIM (CIM containing 40 mg l^{-1} hygromycin, 150 mg l^{-1} timentin) and incubated in the dark at 24 °C for 16 d. Calli were then transferred to selective plant regeneration medium (PRM) containing 4.3 g l^{-1} MS salts, pH 5.8, 10 ml l^{-1} 100× MS vitamins, 20 g l^{-1} sucrose, 7 g l^{-1} Phytoblend, 2 mg l^{-1} kinetin, 150 mg l^{-1} timentin, 15 mg l^{-1} hygromycin. Calli were maintained at 24 °C under a 16 h light:8 h dark photoperiod and a light

intensity of 60 µmol photons m^{-2} s^{-1}. Developing shoots were transferred to selective rooting medium (RM) containing 2.15 g l^{-1} MS salts, pH 5.7, 10 ml l^{-1} 100× MS vitamins, 30 g l^{-1} sucrose, 7 g l^{-1} Phytoblend, 150 mg l^{-1} timentin, 20 mg l^{-1} hygromycin. Shoots that survived and developed roots were genotyped using primers against the hygromycin phosphotransferase gene (Supplementary Table S1) by PCR, and positive transformants were transplanted to soil.

Selection of plants for analysis

The progeny of three independent T_0 transformation events were analysed for CA hydration rates (Supplementary Fig. S1). One T_1 plant with low CA hydration rates was selected from each transformation event (labelled 5.3, 2.1, and 1.1) and its progeny (T_2) used for all future analysis. Two sets of experiments were performed on the T_2 plants. First, gas exchange and biochemical analysis on lines 5.3, 2.1, and 1.1 (Table 1) and, secondly, gas exchange and oxygen discrimination on lines 5.3 and 1.1 (Table 2). Each T_2 plant was genotyped prior to experiments using primers against the hygromycin phosphotransferase gene (Supplementary Table S1). The progeny of a plant which went through the *S. viridis* transformation process and tested negative for the hygromycin phosphotransferase gene were used as null controls.

Insertion number estimation

DNA was isolated from a fully expanded leaf using a CTAB (cetyltrimethylammonium bromide) extraction buffer [2% CTAB (v/v), 20 mM Tris–HCl pH 8, 1.4 M NaCl, 20 mM EDTA, 1% polyvinylpyrrolidone (PVP)-40 (w/v), 0.2% (v/v) β-mercaptoethanol] followed by extraction with phenol/chloroform/isoamylalcohol (25:24:1) and ethanol clean-up. DNA quality and quantity was determined using a NanoDrop spectrophotometer (Thermo Scientific).

IDNA genetics (UK) performed quantitative real-time PCR (qPCR) analysis to estimate the numbers of transgene copies in the CA transformed lines following the procedure described in Bartlett *et al.* (2008) with some modifications. The hygromycin phosphotransferase gene (with a FAM reporter) and the internal positive control (IPC, with a VIC reporter) were amplified together in a multiplex reaction (15 min denaturation, then 40 cycles of 15 s at 95 °C and 60 s at 60 °C) in an ABI1900 real-time PCR machine. Fluorescence from the FAM and VIC fluorochromes was measured during each 60 °C step and the Ct values obtained. The difference between the Ct values for the hygromycin phosphotransferase gene and the IPC (the Delta Ct) was used to allocate the assayed samples into groups with the same gene copy number.

RNA extraction and reverse transcription–quantitative PCR (RT–qPCR)

Leaf discs (0.78 cm^2) frozen and stored at −80 °C were lysed using the Qiagen TissueLyser II. RNA was extracted using the Trizol extraction method and in the presence of RNase inhibitor (Ambion). DNA was removed using the TURBO DNA free kit (Ambion), and RNA quantity and quality were determined using a NanoDrop (Thermo Scientific).

RNA (200 ng) was reverse transcribed into cDNA using Qiagen's RT^2 HT First Strand cDNA synthesis kit. RT–qPCR and melt curve analysis were performed on a Viia7 Real-time PCR system using the Power SYBR green PCR Master Mix (Thermo Fisher) according

Table 1. *Physiological and biochemical characteristics of CA transformants under ambient CO_2 conditions*

Net CO_2 assimilation rate (A), stomatal conductance (g_s), mesophyll pCO_2 (C_m), the rate constant of CA hydration (k_{CA}), and enzyme activities were measured from the uppermost, fully expanded leaf of 5-week-old plants grown at 2% CO_2. Gas exchange measurements were made at 25 °C leaf temperature, flow rate at 500 µmol m^{-2} s^{-1}, and irradiance of 1500 µmol photons m^{-2} s^{-1}. Three T_2 plants from three different transformation events were measured.

	A	g_s	C_m	k_{CA}	Rubisco	PEPC	NADP-ME
	µmol m^{-2} s^{-1}	mol m^{-2} s^{-1}	µbar	mol m^{-2} s^{-1} bar^{-1}	µmol m^{-2} s^{-1}	µmol m^{-2} s^{-1}	µmol m^{-2} s^{-1}
Null	22.5 ± 0.6 a	0.19 ± 0.01 a	132.4 ± 3.3 a	6.1 ± 0.8 a	18.7 ± 1.5 a	229.6 ± 19.3 a	59.8 ± 4.3 a
5.3	21.7 ± 2.6 a	0.2 ± 0.02 a	118.9 ± 13.1 a	3.3 ± 0.2 b	18.8 ± 1.8 a	249.3 ± 24.6 a	54.5 ± 5.8 a
2.1	18.5 ± 1.9 a	0.16 ± 0.01 a	152.9 ± 15.2 a	2.0 ± 0.2 b,c	20.9 ± 2.9 a	181.5 ± 25.4 a	47.3 ± 2.6 a
1.1	19.1 ± 1.2 a	0.19 ± 0.02 a	153.9 ± 4.4 a	0.8 ± 0.1 c	19.7 ± 1.8 a	180.3 ± 18.4 a	43.6 ± 3.9 a

Significant differences are based on one-way ANOVA and Tukey post-hoc analysis (SPSS statistics version 22; P=0.05).

Table 2. *Physiological characteristics of CA transformants at ambient CO_2 measured using LI-6400XT coupled to a tunable diode laser*

Net CO_2 assimilation rate (A), stomatal conductance (g_s), mesophyll pCO_2 (C_m), the ratio of intercellular to ambient pCO_2 (C_i/C_a), the rate constant of CA hydration (k_{CA}), online $\Delta^{18}O$ discrimination, and the length of mesophyll cells exposed to intercellular airspace (S_m) were measured on the uppermost, fully expanded leaf of 5-week-old plants grown at 2% CO_2. Gas exchange measurements were made at 2% O_2, 25 °C leaf temperature, flow rate at 500 µmol m^{-2} s^{-1}, and irradiance of 1500 µmol photons m^{-2} s^{-1}. Three T_2 plants from two different transformation events were measured.

	A	g_s	C_m	C_i/C_a	k_{CA}	$\Delta^{18}O$	S_m
	µmol m^{-2} s^{-1}	mol m^{-2} s^{-1}	µbar	µbar	mol m^{-2} s^{-1} bar^{-1}	‰	m^2 m^{-2}
Null	30.0 ± 1.4 a	0.30 ± 0.03 a	144.6 ± 5.9 a	0.39 ± 0.03 a	8.4 ± 0.7 a	18.0 ± 1.4 a	10.2 ± 0.4 a
5.3	29.2 ± 0.9 a	0.29 ± 0.02 a	157.9 ± 10.5 a	0.34 ± 0.01 a	2.5 ± 0.3 b	13.6 ± 0.7 a,b	–
1.1	24.5 ± 1.6 a	0.26 ± 0.03 a	178.1 ± 13.5 a	0.43 ± 0.02 a	0.8 ± 0.2 b	10.9 ± 0.6 b	10.2 ± 0.9 a

Significant differences are based on one-way ANOVA and Tukey post-hoc analysis (SPSS statistics version 22; P=0.05).

to the manufacturer's instructions. Primers (Supplementary Table S1) were designed using Primer3 in Geneious R7.1.6, ensuring products spanned an intron. Primer amplification efficiencies were determined by the Ct slope method; efficiencies for all primer pairs were comparable (~95%) and no amplification was detected in the no template control. Relative fold change was calculated by the ΔΔCt method, using the average of three nulls as reference, as described by Livak and Schmittgen (2001). The geometric mean of the Ct values for three reference genes was used for normalization (Vandesompele *et al.*, 2002). Statistics were performed with SigmaPlot (version 11.0).

Determination of enzyme activities

For CA activity, leaf discs (0.78 cm^2) were collected from the uppermost fully expanded leaf of 5-week-old *S. viridis* plants and frozen in liquid nitrogen. Soluble protein was extracted by grinding one frozen leaf disc in ice-cold glass homogenizers (Tenbroek) in 500 µl of extraction buffer [50 mM HEPES, pH 7.8, 1% (w/v) PVP, 1 mM EDTA, 10 mM dithiothreitol, 0.1% (v/v) Triton X-100, 2% (v/v) protease inhibitor cocktail (Sigma)]. Crude extracts were centrifuged at 4 °C for 1 min at 13 000 *g* and the supernatant collected for the soluble CA assay. Activity was measured on a membrane inlet mass spectrometer to measure the rates of ^{18}O exchange from labelled $^{13}C^{18}O_2$ to $H_2{}^{16}O$ at 25 °C (Badger and Price, 1989; von Caemmerer *et al.*, 2004). The hydration rates were calculated as described by Jenkins *et al.* (1989).

For Rubisco, PEPC, and NADP-malic enzyme (ME) activities, soluble protein was extracted from fresh leaf discs collected from leaves used for gas exchange analysis. Spectrophotometric assays were then performed as described previously (Pengelly *et al.*, 2010, 2012; Sharwood *et al.*, 2016).

Gas exchange measurements

Net photosynthesis (A) was measured over a range of intercellular pCO_2 (C_i) on the uppermost, fully expanded leaf of 5-week-old *S. viridis* plants using a portable gas exchange system LI-COR 6400XT (LI-COR Biosciences). Measurements were made after leaves had equilibrated at 380 µbar, flow rate 500 µmol s^{-1}, leaf temperature 25 °C, and irradiance 1500 µmol photons m^{-2} s^{-1}. CO_2 response curves were measured in a stepwise increase (3 min intervals) in CO_2 partial pressure 380, 0, 23.75, 47.5, 71.25, 95, 142.5, 190, 285, 380, 570, 760, and 950 µbar whilst maintaining leaf temperature and irradiance conditions.

Measurements of $C^{18}O^{16}O$ discrimination ($\Delta^{18}O$)

Simultaneous measurements of exchange of CO_2, H_2O, $C^{18}O^{16}O$, and $H_2{}^{18}O$ were made by coupling two LI-6400XT gas exchange systems to a tunable diode laser (TDL: TGA200A, Campbell Scientific Inc., Logan, UT, USA) to measure $C^{18}O^{16}O$ and a Cavity Ring-Down Spectrometer (L2130-i, Picarro Inc., Sunnyvale, CA, USA) to measure the oxygen isotope composition of water vapour. The system is essentially that described by Tazoe *et al.* (2011) except that the TGA100 was replaced by a TGA200A and the additional laser for water vapour measurements has been added together with a 16 port distribution manifold. To generate gas flows to the gas exchange systems, N_2 and O_2 were mixed by mass flow controllers (Omega Engineering Inc., Stamford, CT, USA) to generate CO_2-free air with 2% O_2. The humidity of incoming air was adjusted by varying the temperature of water circulating around a Nafion tube (Permapure, MH-110-12P-4) but was kept constant in this set of experiments to supply water vapour of a constant ^{18}O composition. To supply flow to the TDL and the L2130-i from the sample and reference gas streams, two T junctions were inserted into the match valve tubing and in the reference line of the LI-6400XT, respectively. This allowed leaves of two plants to be measured in sequence, with each LI-6400XT sampled by the TDL at 4 min intervals for 20 s at the sample and reference line. The Picarro Cavity Ring Down spectrometer sampled for 3 min, so that leaves were sampled at 6 min intervals.

Supplementary Fig. 5 shows the CO_2 dependence of the standard error of $\delta^{18}O$ of CO_2 in the reference gas of repeated measurements on the TGA200A. The ^{18}O isotopic composition of the CO_2 calibration gas was 22.17 ± 0.04‰ for Vienna mean oceanic water (VSMOW) and was checked against standards on an Isoprime mass spectrometer. We monitored the ^{18}O composition of water vapour of the reference air streams daily, and the values were −6.07 ± 0.08‰ and −6.34 ± 0.08‰ (VSMOW) for LI-6400XT L1 and L2 references, respectively. We attribute the small difference between the reference lines to differences in the Nafion tubing. At the end of the experiment, the calibration of the Picarro L2130-i was confirmed by collecting water vapour samples from the gas stream of the LI-6400XT reference lines going to the Picarro as described by Cousins *et al.* (2006) and assaying these water samples against standards on a Picarro 1102i, which was set up to measure the ^{18}O isotopic composition of water samples.

Gas exchange was measured on the uppermost fully expanded leaf of 5-week-old *S. viridis* plants at 25 °C, and leaves were equilibrated at ambient CO_2 (380 µbar), irradiance 1500 µmol photons m^{-2} s^{-1}, and 2% O_2. The flow rate was 200 µmol s^{-1}. CO_2 concentration was adjusted from 380 to 760, 570, 380, and 190 µbar at 1 h intervals. Immediately following gas exchange measurements, leaf discs were collected and stored at −80 °C until measurements of CA activity were made.

Calculations of $C^{18}O^{16}O$ ($\Delta^{18}O$) discrimination and mesophyll conductance (g_m)

Discrimination against ^{18}O in CO_2 during photosynthesis, $\Delta^{18}O$, was calculated from the isotopic composition of the CO_2 entering δ_{in} and exiting δ_{out} the leaf chamber and the CO_2 concentration entering C_{in} and exiting C_{out} (all measured with the TDL) (Evans *et al.*, 1986; Barbour *et al.*, 2016;):

$$\Delta^{18}O = \frac{\xi(\delta_{out} - \delta_{in})}{1 + \delta_{out} - \xi(\delta_{out} - \delta_{in})} \quad (1)$$

where $\xi = C_{in}/C_{in} - C_{out}$. Sample streams were passed through a Nafion drying tube before entering the TDL, and CO_2 values presented are all at zero water vapour concentration.

Following the derivation by Barbour *et al.* (2016) and Farquhar and Cernusak (2012) photosynthetic $\Delta^{18}O$ discrimination was used to calculate pCO_2 in the mesophyll cytosol, C_m, with the assumption that C_m is equal to the pCO_2 at the site of CO_2–H_2O exchange and assuming that cytosolic CO_2 is in full isotopic equilibrium with local cytosolic water. This allowed g_m to be calculated from

$$g_m = A / (C_i - C_m) \quad (2)$$

$$C_m = C_i \left(\frac{\delta_i - a_w - \delta_A (1 + a_w)}{\delta_c - a_w - \delta_A (1 + a_w)} \right) \quad (3)$$

Equation 3 is the same as equation 21 of Barbour *et al.* (2016), and is a rearrangement of equation 18 of Farquhar and Cernusak (2012) using their notation. The oxygen isotope ratios are expressed relative to the standard, (VSMOW) $\left(\delta_x = \frac{\left(^{18}O / {}^{16}O\right)_x}{\left(^{18}O / {}^{16}O\right)_{std}} - 1\right)$. Intercellular pCO_2 is denoted by C_i, and a_w is the discrimination against $C^{16}O^{18}O$ during liquid phase diffusion and dissolution (0.8‰).

The isotopic composition of CO_2 being assimilated, δ_A, is given by

$$\delta_A = \frac{\delta_a - \Delta^{18}O}{1 + \Delta^{18}O}, \quad (4)$$

where δ_a is the isotopic composition of ambient air (in our case $\delta_a=\delta_{out}$).

The oxygen isotope composition of CO_2 in the intercellular airspaces, δ_i, including ternary corrections proposed by Farquhar and Cernusak (2012), is given by

$$\delta_i = \frac{\delta_{io} + t\left[\delta_A\left(\frac{C_a}{C_i}+1\right) - \delta_a\frac{C_a}{C_i}\right]}{1+t} \quad (5)$$

where C_a is the pCO_2 in the ambient air. The ternary correction factor, t, is given by

$$t = \frac{\left(1+\frac{a_{18bs}}{1000}\right)E}{2g_{ac}} \quad (6)$$

where g_{ac} is the total conductance to CO_2, E the transpiration rate, and a_{18bs} is the weighted discrimination of $C^{16}O^{18}O$ diffusion across the boundary layer and stomata in series given by:

$$a_{18bs} = \frac{(C_a - C_s)a_{18b} - (C_s - C_i)a_{18s}}{(C_a - C_i)} \quad (7)$$

where C_s is the pCO_2 at the leaf surface and a_{18s} and a_{18b} are the discriminations against $C^{16}O^{18}O$ through stomata and the boundary layer (8‰ and 5.8‰, respectively).

The isotopic composition of intercellular CO_2 ignoring ternary corrections is given by

$$\delta_{io} = \delta_A\left(1-\frac{C_a}{C_i}\right)(1+a_{18bs}) - \frac{C_a}{C_i}(\delta_a - a_{18bs}) + a_{18bs} \quad (8)$$

To calculate C_m, we assume that the isotopic composition of CO_2 in the cytosol, δ_c, is the isotopic composition of CO_2 equilibrated with cytosolic water, δ_{cw}, and

$$\delta_{cw} = \delta_w + \varepsilon_w \quad (9)$$

where δ_w is the stable oxygen isotope composition of water in the cytosol at the site of evaporation and ε_w is the isotopic equilibrium between CO_2 and water (dependent on temperature T_K in K (Barbour *et al.*, 2016, and references therein).

$$\varepsilon_w(‰) = \frac{17604}{T_K} - 17.93 \quad (10)$$

Calculation of the isotopic composition of water at the site of evaporation from the isotopic composition of transpired water

The isotopic composition of water at the site of evaporation, δ_w, can be estimated from the Craig and Gordon model of evaporative enrichment (Craig and Gordon, 1965; Farquhar and Lloyd, 1993)

$$\delta_w = \delta_t + \varepsilon^* + \varepsilon_k + \frac{e_a}{e_i}(\delta_{wa} - \varepsilon_k - \delta_t) \quad (11)$$

where ε^* is the equilibrium fractionation during evaporation, ε_k is the kinetic fractionation during vapour diffusion in air, δ_t is the oxygen isotopic composition of transpired water, e_a/e_i is the ratio of ambient to intercellular vapour pressure, and δ_a is the isotopic composition of ambient air. ε^* is dependent on temperature:

$$\varepsilon^* = 2.644 - 3.206\left(\frac{10^3}{T_K}\right) + 1.534\left(\frac{10^6}{T_K^2}\right) \quad (12)$$

ε_k is dependent on stomatal and boundary layer conductances and associated fractionation factors (Barbour *et al.*, 2016, and references therein):

$$\varepsilon_k = \frac{28g_s^{-1} + 19g_b^{-1}}{g_s^{-1} + g_b^{-1}} \quad (13)$$

The isotopic composition of transpired water δ_t can be calculated from mass balance knowing the isotopic composition of the water entering δ_{win} and exiting δ_{wout} the leaf chamber (measured with the Picarro) and the water vapour concentration entering w_{in} and exiting w_{out} (measured with the LI-6400XT):

$$\delta_t = \left(\delta_{wout}(1-w_{in}) - \delta_{win}\frac{w_{in}}{w_{out}}(1-w_{out})\right)\frac{w_{out}}{w_{out}-w_{in}} \quad (14)$$

Calculation of the proportion of mesophyll cytosolic CO_2 in equilibration with leaf water, θ

If C_m is known, it is possible to calculate the isotopic composition of cytosolic CO_2 from measurements of $\Delta^{18}O$ using equation 18 from Farquhar and Cernusak (2012):

$$\delta_c = \delta_A\left(1-\frac{C_i}{C_m}\right)(1+a_w) + \frac{C_i}{C_m}(\delta_i - a_w) + a_w. \quad (15)$$

This can then be compared with δ_{cw} (Equation 9), the isotopic composition of CO_2 in equilibrium with water at the site of evaporation. We calculated mesophyll conductance, g_m, in the *S. viridis* null plants assuming that $\delta_c=\delta_{cw}$ and then used this g_m to estimate C_m in the *S. viridis* transgenics to calculate the proportion of cytosolic CO_2 in equilibration with leaf water, θ using equations developed by Cernusak *et al.* (2004)

$$\theta = \frac{\delta_c - \delta_a + a_{18}\left(1+\frac{C_c}{C_a}\right)}{\delta_{cw} - \delta_a + a_{18}\left(1+\frac{C_c}{C_a}\right)} \quad (16)$$

where a_{18} is the weighted discrimination of $C^{16}O^{18}O$ diffusion across the boundary layer, stomata, and the liquid phase in series given by:

$$a_{18} = \frac{a_b(C_a - C_s) + a_s(C_s - C_i) + a_w(C_i - C_m)}{(C_a - C_m)}. \quad (17)$$

Leaf anatomical measurements and estimation of g_m from anatomical measurements

Fully expanded leaves from 5-week-old T_2 plants, null and line 1.1, were collected and cut into ~0.5 × 2 mm pieces. Leaf slices were fixed in 2.5% (v/v) glutaraldehyde, 2% (v/v) paraformaldehyde, 0.1 M phosphate buffer, and 0.01% (v/v) Tween-20 under vacuum for 20 min, then replaced with buffer containing no Tween-20 and fixed overnight at 4 °C. Leaf pieces were washed in phosphate buffer and post-fixed in 1% (w/v) osmium tetroxide for 2 h. Fixed leaf pieces were then dehydrated in an ethanol series (10, 30, 50, 70, 80, 95, 100%) followed by infiltration with LR white. Leaf sections were finally placed in moulds filled with resin and baked at 60 °C for 24 h. Sections of 0.5 µm thickness were cut using glass knives on a Reichert ultramicrotome, stained with toluidine blue, and heat fixed to glass slides. Slides were viewed using a Zeiss Axioskop light microscope at ×400 magnification. Three images were taken from each slide for analysis, each containing a leaf cross-section in the same orientation and showing at least two vascular bundles. Fiji quantification

software (Schindelin *et al.*, 2012) was used to select regions of interest. Mesophyll surface area exposed to intercellular airspace to leaf area ratio (S_m) was calculated using Equation 18 where CCF is the curvature correction factor of 1.43 (Evans *et al.*, 1994).

$$S_m = \frac{\text{Length of mesophyll cells exposed to intercellular airspace}}{\text{Interveinal distance}} \times \text{CCF} \quad (18)$$

The values of S_m together with measurements of cell wall thickness and cytosol thickness were used to derive an estimate of g_m from anatomical parameters. The cell wall thickness (0.113 ± 0.005 µm) was kindly estimated from transmission electron micrographs of *S. viridis* grown under similar conditions by Florence Danila (Danila *et al.*, 2016). Calculations followed equations 1–5 of von Caemmerer and Evans (2015) using the membrane permeability of Gutknecht for a lipid bilayer of 3.5×10^{-3} m s^{-1} since only the plasma membrane needs to be transversed for diffusion of CO_2 from he intercellular airspace to mesophyll cytosol (Gutknecht *et al.*, 1977) and a cytosol thickness of 0.3 µm (von Caemmerer and Evans, 2015). These calculations give a g_m of 0.68 mol m^{-2} s^{-1} bar^{-1}.

Statistical analysis

One-way ANOVAs with post-hoc Tukey test analyses were performed for all measurements of gas exchange and enzyme activities with P=0.05 using the IBM SPSS Statistics 22 package.

Results

Generation of transgenic S. viridis *with reduced β-CA*

In *S. viridis* we identified four β-CA genes: Si002140m.g (with one other isoform Si002148m), Si002669m.g, Si030616m.g (with two other isoforms Si030928m and Si030803m), and Si003882m.g. There is very low sequence identity between these β-CA genes, ~37% (Supplementary Fig. S2). Si003882m.g has been shown to be the major leaf β-CA (Christin *et al.*, 2013; John *et al.*, 2014).

Three independent transformation events resistant to hygromycin and with reduced CA activity were generated using two different approaches. First, one line (1.1) was generated through gene suppression upon transformation with the overexpression construct pSC110/*ZmCA2*. The coding sequences of *ZmCA2* and Si003882m.g show 87% identity (Supplementary Fig. S3). Most probably, expression of *ZmCA2* therefore caused suppression of the primary *S. viridis* β-CA gene, resulting in reduced CA activity in line 1.1. The second approach was to target Si003882m.g using the RNAi construct pSG/*CAa* which generated stably transformed lines from two different events (2.1 and 5.3). Plants were grown at high pCO_2 for all experiments.

To determine the specificity of the RNAi construct and check which β-CA was suppressed in line 1.1, RT–qPCR was performed against the β-CAs in *S. viridis*. Expression of the primary leaf β-CA Si003882m.g was significantly down-regulated, between 83% and 96%, in lines from all three transformation events (Fig. 1A). Transcript levels of Si030616m.g and Si002140m.g were unchanged relative to expression in the null plants (Fig. 1B, C) while Si002669m.g transcript was undetectable in all samples (data not shown). Therefore, expression of only the target β-CA gene was affected in the three transformed lines.

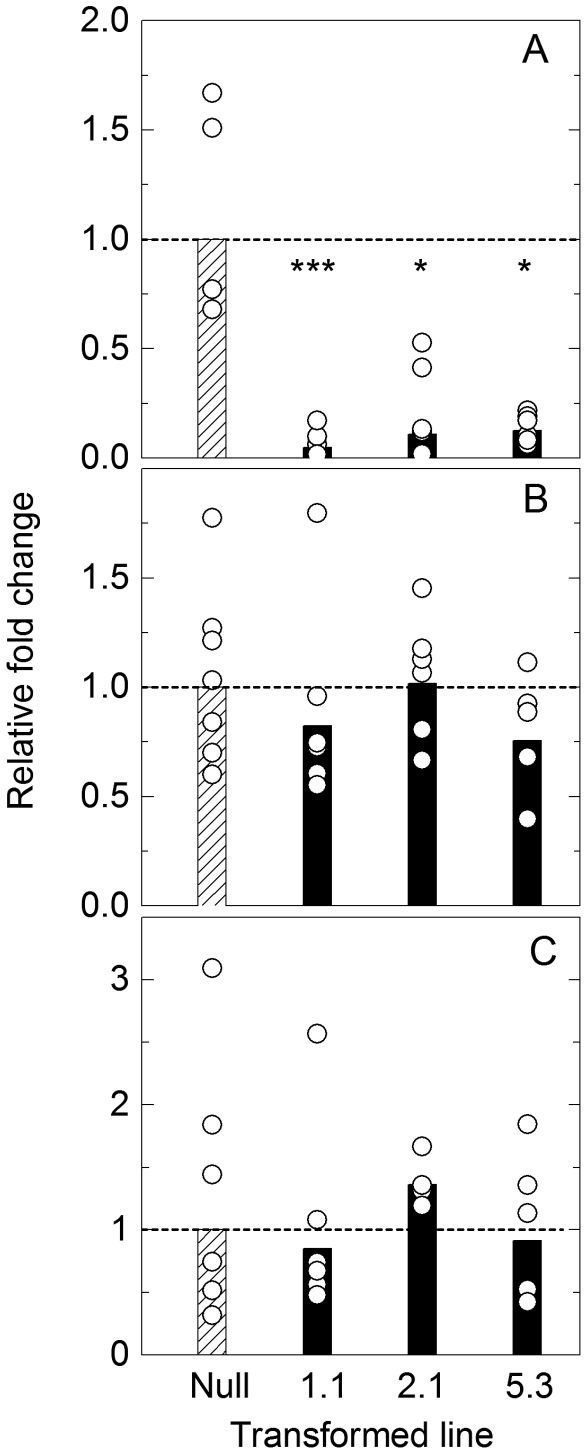

Fig. 1. Expression level of β-CA transcripts. (A) Si003882m.g, (B) Si002140m.g, and (C) Si030616m.g in null control and CA transformed lines 1.1, 2.1, and 5.3 as measured by RT–qPCR and analysed by ΔΔCt. Fold change relative to the null transformant is shown; bars represent mean fold change, and circles show the data range of T_2 plants (n=5–7 plants) from each transformation event measured in triplicate. The dotted line indicates average null fold change. Expression level of the major leaf β-CA transcript Si003882m.g (A) is significantly lower compared with the null control in all three transformed lines, calculated using one-way ANOVA.

qPCR was used to estimate the number of insertions in the transgenic plants, based on the number of copies of the hygromycin phosphotransferase gene. Three T_2 plants of the

three lines were analysed and there were two, four, and more than four transgene insertions detected for plants of line 5.3, 2.1, and 1.1, respectively. The high copy number in the over-expressing line of 1.1 is the likely cause of the suppression of transcript accumulation.

CA and photosynthetic enzyme activity and leaf anatomy

T_1 progeny of the three independent transformation events showed a range of CA hydration rates as measured on the soluble leaf fraction on a membrane inlet mass spectrometer. Compared with the null control, lines 1.1, 2.1, and 5.3 had on average (n=7 T_2 plants) an 87, 70, and 50% reduction of CA activity, respectively (Fig. 2). The CA hydration rate in the null plants was 934 ± 92 µmol m^{-2} s^{-1} as calculated at a mesophyll pCO_2 (C_m) of 140 µbar (Equation 2).

The activities of the photosynthetic enzymes Rubisco, PEPC, and NADP-ME were unchanged in lines 5.3, 2.1, and 1.1 compared with the nulls (Table 1) and showed no correlation with CA hydration rates (one-way ANOVA and Tukey post-hoc analysis (SPSS statistics version 22; P=0.05).

No significant differences were observed for the surface area of mesophyll cells exposed to intercellular airspace per unit leaf area (S_m) in embedded leaf sections of nulls (10.22 ± 0.35 m^2 m^{-2}) and plants from line 1.1 (10.18 ± 0.95 m^2 m^{-2}). These anatomical measurements were used to estimate an anatomical g_m of 0.68 mol m^{-2} s^{-1} bar^{-1} (see the Materials and methods).

CA activity and CO_2 assimilation rates

The response of CO_2 assimilation rate (A) to increasing intercellular pCO_2 (C_i) was investigated to examine the effect of reduced CA activity on CO_2 assimilation rates (Fig. 3). There were no statistical differences in the maximum rate of CO_2 assimilation under ambient or high CO_2 conditions between null control and progeny of transformant lines. At low pCO_2, CO_2 assimilation rates were reduced to varying degrees in the progeny of the transformed lines compared with the null control. Individuals of line 1.1 with the lowest CA hydration rate had the lowest initial slopes of the AC_i curves.

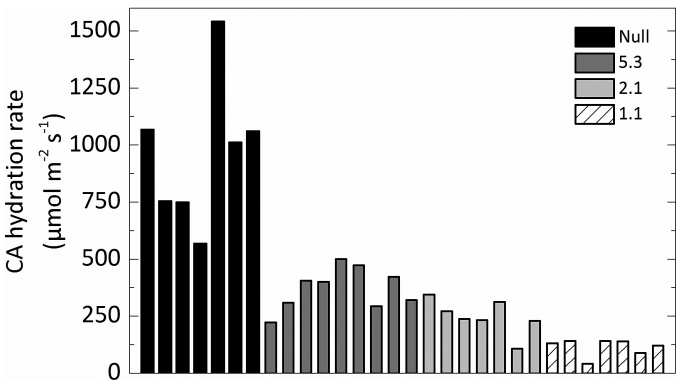

Fig. 2. Range of CA hydration rates at mesophyll pCO_2 (C_m) measured using a membrane inlet mass spectrometer in the null control and T_2 plants from lines 5.3, 2.1, and 1.1.

The initial slopes of the AC_i and AC_m curve were plotted against the CA hydration rate constant (k_{CA}; Fig. 4). Mesophyll cytosolic pCO_2, C_m, was calculated from Equation 2, using the average null g_m (0.9 mol m^{-2} s^{-1} bar^{-1}) since there was no difference in S_m. A strong correlation between the initial slope from the AC_m curve and k_{CA} was observed, with the initial slope increasing as CA hydration rates increase (R^2=0.845; Fig. 4). There was a curvilinear response between the initial slope of the AC_i curves indicating other limitations. No difference in stomatal conductance (g_s) was observed across a range of intercellular pCO_2 between null controls and any of the transformed lines during the rapid measurements of CO_2 responses (Fig. 5).

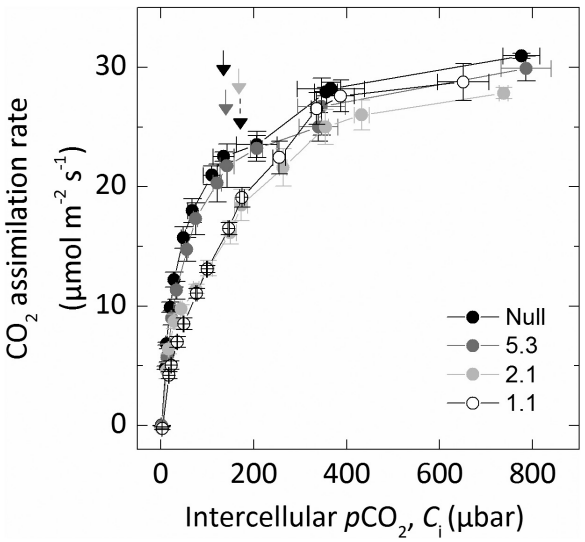

Fig. 3. CO_2 assimilation rate of transformed lines over a range of intercellular pCO_2 (C_i). Average of three T_2 plants from each line. Plants were grown at 2% CO_2, and the uppermost, fully expanded leaves of 5-week-old plants were measured using a LI-6400XT at 25 °C leaf temperature at an irradiance of 1500 µmol photons m^{-2} s^{-1}. Arrows mark ambient pCO_2 for each line; note that the dotted arrow is line 1.1.

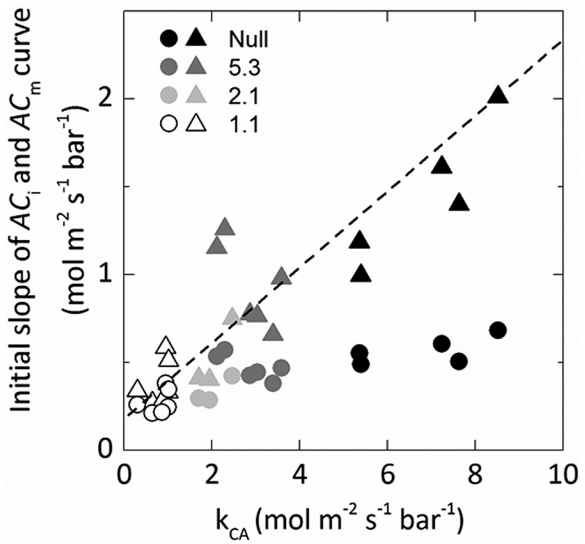

Fig. 4. Relationship between the initial slope of the AC_m (triangles) or AC_i (circles) curves and the rate constant of CA hydration rates (k_{CA}), AC_m R^2=0.846. Each point represents a measurement made on an individual leaf of a T_2 plant.

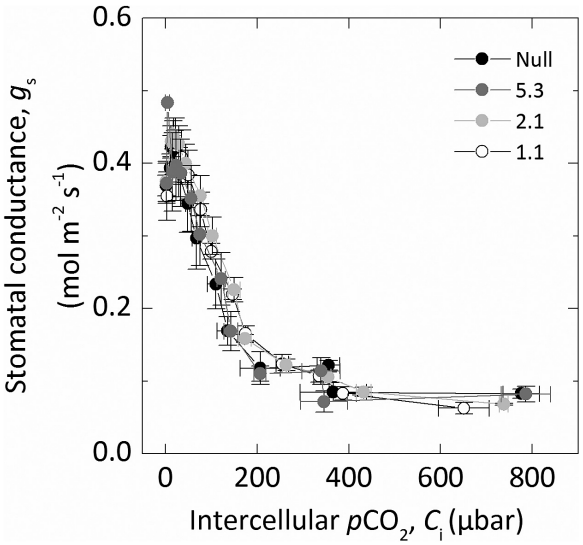

Fig. 5. Stomatal conductance (g_s) over a range of intercellular pCO_2 (C_i). Measurements were made concurrently with those in Fig. 4.

Oxygen isotope discrimination measurements

Oxygen ($\Delta^{18}O$) isotope discrimination and CO_2 assimilation rates were measured in response to changes in pCO_2 using a LI-6400XT coupled to a TDL trace gas analyser to measure $C^{18}O^{16}O$ and a Cavity Ring-Down Spectrometer to measure the oxygen isotope composition of water vapour. Transformed plants with reduced CA hydration rates had lower $\Delta^{18}O$ compared with the nulls, but only line 1.1 was significantly lower (Table 2).

In the null controls, measurements of $\Delta^{18}O$ were used to estimate conductance of CO_2 from the intercellular airspace to the sites of CO_2 and H_2O exchange in the cytosol (g_m) with the assumption that CO_2 was in full isotopic equilibrium with leaf water in the cytosol (Equation 2; Fig. 6). Although g_m appeared to increase with decreasing C_i, there were no significant differences between g_m estimated at the different C_i, and the average value was 0.94 ± 0.06 mol m^{-2} s^{-1} bar^{-1} (Fig. 6B). C_i–C_m indicates the drawdown of CO_2 from the intercellular airspace to the site of fixation, and for the null controls there is an increasing gradient of pCO_2 as C_i increases (Fig. 6C).

$\Delta^{18}O$ at ambient pCO_2 showed statistically significant differences between line 1.1 (with the lowest CA activity) and null plants (Table 2). When plotted against C_m/C_a, $\Delta^{18}O$ measurements closely correspond to theoretical curves representing θ (Equation 16) under different scenarios either where cytosolic CO_2 is at full isotopic equilibrium with the cytosolic water (null lines) or where there is only partial equilibrium (such as line 1.1; Fig. 7). Calculated values for line 5.3 which showed a 50% reduction in CA activity relative to the null controls fell in between these two theoretical lines. This is illustrated again with theta (θ) of lines 1.1 and 5.3 over a range of C_m (Fig. 8). When CO_2 is at full isotopic equilibrium with the cytosolic water, θ would be 1, whereas in lines 1.1 and 5.3 (with reduced CA hydration rates relative to the null control) θ is <1. There was no CO_2 dependence of θ over the range of pCO_2 measured.

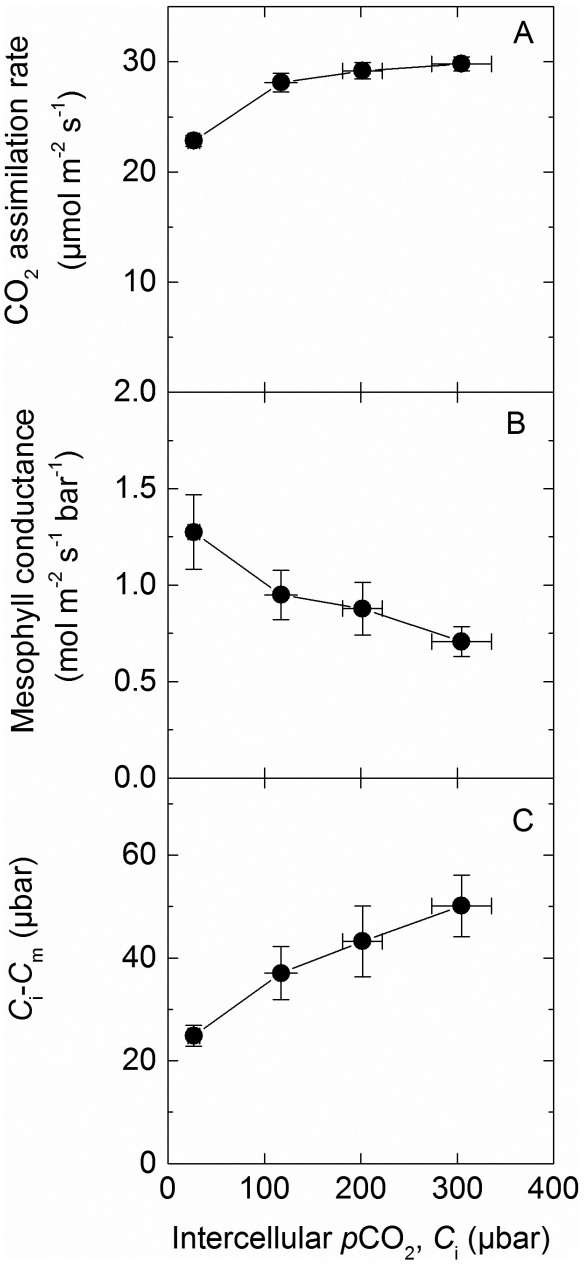

Fig. 6. (A) CO_2 assimilation rate, (B) mesophyll conductance (g_m; Equation 2), and (C) C_i–C_m over a range of intercellular pCO_2 in null controls measured using a LI-6400XT coupled to a tunable diode laser. Plants were grown at 2% CO_2 and the uppermost, fully expanded leaves of 5-week-old plants were measured at 25 °C leaf temperature, flow rate 200 µmol m^{-2} s^{-1}, 2% O_2 at an irradiance of 1500 µmol photons m^{-2} s^{-1}.

Discussion

Setaria viridis *as a model species to study photosynthetic physiology in a C_4 monocot*

Flaveria bidentis, a readily transformable model C_4 dicot, has been successfully used to study the regulation of C_4 photosynthesis using antisense and RNAi technology (Furbank *et al.*, 1997; Matsuoka *et al.*, 2001; von Caemmerer *et al.*, 2004; Pengelly *et al.*, 2012). This work has been crucial in quantifying the rate-limiting steps in the C_4 pathway by 'titrating' out levels of target enzymes by gene suppression and observing

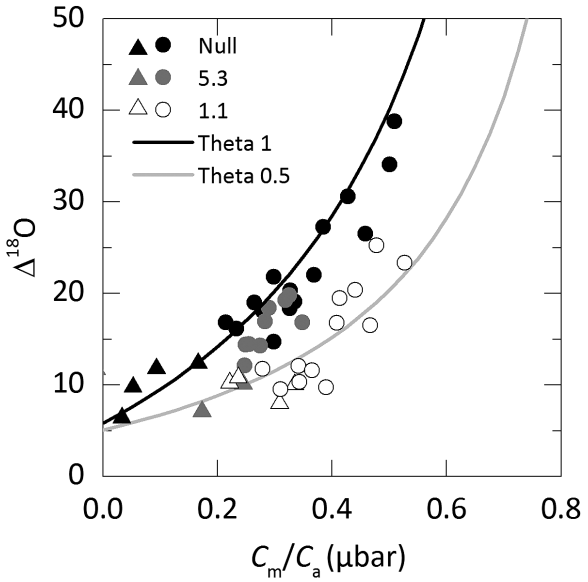

Fig. 7. Oxygen isotope discrimination ($\Delta^{18}O$) as a function of the ratio of mesophyll pCO_2 to ambient pCO_2 (C_m/C_a) in null and lines 5.3 and 1.1. Each point represents a measurement made on an individual leaf of a T_2 plant. Triangular symbols represent measurements made at low pCO_2. Theoretical curves represent the scenario where cytosolic CO_2 is at full isotopic equilibrium with cytosolic water (θ=1, black) or under partial equilibrium (θ=0.5, grey) of ^{18}O in the leaf. The equations for the curves are given by $\Delta^{18}O = a_{18} + \frac{C_m}{C_a - C_m}(\delta_c - \delta_a)$ and a_{18}=5.85‰ and δ_c–δ_a=33‰ at full equilibration or a_{18}=5.1‰ and δ_c–δ_a=15‰ (Farquhar and Lloyd, 1993).

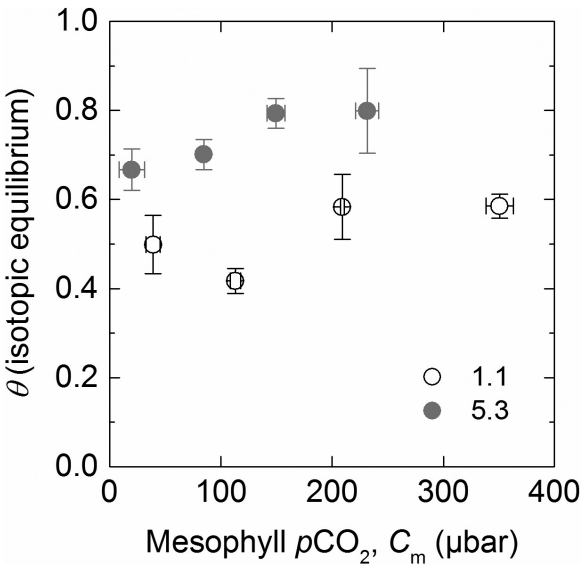

Fig. 8. Average isotopic equilibrium (theta, θ) over a range of mesophyll pCO_2 in two reduced CA lines 5.3 (grey) and 1.1 (white). Measured values of θ were determined from $\Delta^{18}O$ using Equation 16. Each point represents the average measurement of three T_2 plants.

the effects on physiological characteristics of the resultant transgenics (Furbank *et al.*, 1997). There are, however, important differences between C_4 dicots and the C_4 monocots which make up the majority of agriculturally important C_4 species. *Setaria viridis* has emerged as a new model grass to study C_4 photosynthesis in crops and related bioenergy species. *Setaria viridis* is an appropriate biochemical model species for *Z. mays* and *S. bicolor* as all three use NADP-ME as the primary decarboxylation enzyme. We generated transgenic *S. viridis* plants with reduced CA activity to compare the effect with previous results obtained with *F. bidentis* and *Z. mays* (von Caemmerer *et al.*, 2004; Studer *et al.*, 2014) and to explore the effect that a reduction in CA activity has on the initial slope of the AC_i and AC_m curves. In these lines, only the major leaf isoform of β-CA was reduced (Fig. 1). The transgenic plants had a range of different CA activities (Fig. 2), but showed no changes in PEPC and Rubisco activity (Table 1) or anatomical parameters (Table 2), making these plants ideal for exploring the role of CA activity in *S. viridis*.

Initial slope of AC$_i$ curves in C$_4$ plants

Models of C_4 photosynthesis suggest that the initial slope of the AC_i curve is determined by three possible limitations: (i) the mesophyll conductance to CO_2 diffusion from the intercellular airspace to the mesophyll cytosol (g_m); (ii) the rate of CO_2 hydration by CA; and (iii) the rate of PEP carboxylation (von Caemmerer, 2000). However, it is not readily known which is the major limitation in C_4 species. Studies with PEPC mutants from the C_4 dicot *Amaranthus edulis* indicate that PEPC activity may not be the major limitation as a 60% reduction in PEPC leads to only a 20% reduction in the CO_2 assimilation rate at ambient pCO_2 accompanied by a small reduction in initial slope for the AC_i curves (Dever *et al.*, 1992; Dever, 1997; Cousins *et al.*, 2007). This study with *S. viridis* confirms that substantial reductions in CA activity are possible before a reduction in steady-state CO_2 assimilation rate and initial slope of the AC_i curve are observed. This is in accordance with previous observations in *F. bidentis* and *Z. mays* (von Caemmerer *et al.*, 2004; Studer *et al.*, 2014).

The Michaelis–Menten constant for CO_2 for CA is >2 mM (~5% CO_2) which makes it appropriate to quantify CA activity by its first-order rate constant (Jenkins *et al.*, 1989; Hatch and Burnell, 1990) and simplifies species comparisons. In *S. viridis*, the lowest rate constant recorded was 0.8 mol m^{-2} s^{-1} bar^{-1} compared with values of 0.1 for the *ca1ca2* double mutant in *Z. mays* and 0.47 for transgenic *F. bidentis* (von Caemmerer *et al.*, 2004; Studer *et al.*, 2014). With this low rate constant, *F. bidentis* had very low CO_2 assimilation rates and the CO_2 response curves did not saturate at high CO_2. In contrast, for both *S. viridis* transgenics and *Z. mays* mutants, CO_2 assimilation rates were only slightly less than in the controls, suggesting that *S. viridis* is more similar to *Z. mays* in its CA requirements. This suggests that these two monocot species can make better use of leaf CA activity or that *in vivo* CA activity is greater than that estimated *in vitro*.

Mesophyll conductance and the initial slope of AC$_m$ curves

Next, we used recently established techniques that utilize ^{18}O discrimination measurements to quantify g_m in our null controls (Fig. 6B; Barbour *et al.*, 2016). This estimates the

diffusion of CO_2 from the intercellular airspace through the cell wall, plasma membrane, and cytosol to the sites of CA activity. At ambient pCO_2, the g_m observed for the null plants were similar to those reported by Barbour *et al.* (2016). A key assumption for the calculation of g_m is that CA activity is not limiting and that CO_2 is in isotopic equilibrium with HCO_3^-; consequently g_m was not measured in the transgenic lines with reduced CA activity. In C_3 species, g_m (in this instance from the intercellular airspace to the chloroplast stroma) has been shown to be proportional to the chloroplast surface area appressing the intercellular airspace per unit leaf area (Evans *et al.*, 1994). Evans and von Caemmerer (1996) hypothesized that in C_4 species g_m may correlate with the mesophyll surface area exposed to intercellular airspace per unit leaf area (S_m). Since S_m was similar between the nulls and line 1.1 plants, we assumed that g_m may also be similar between the plants. In C_3 species, g_m has been shown to, in some instances, increase with decreasing pCO_2 (Flexas *et al.*, 2007; Tazoe *et al.*, 2011; Alonso-Cantabrana and von Caemmerer, 2016). These changes to g_m which may be important in regulating and maintaining photosynthesis were also observed here in the *S. viridis* null plants, with g_m increasing slightly at low pCO_2. However, because the differences in g_m at different pCO_2 were not significant, we used the average g_m estimated for the null plants to calculate mesophyll cytosolic pCO_2 (C_m) in the transgenics.

As shown in Fig. 4, a strong almost linear relationship was found between AC_m and k_{CA}, whereas a saturating relationship was observed with AC_i. This indicates that the CO_2 assimilation rate is limited by cytosolic CA activity, with the relationship becoming clearer after accounting for g_m. It is tempting to speculate that the differences between the two monocot species and *F. bidentis* relate to differences in limitations imposed by g_m which affects cytosolic pCO_2 and hence *in vivo* CA activity, but this is not borne out by comparative measurements of g_m made by Barbour *et al.* (2016). CA activity increases with increasing pH, so variation in cytosolic pH can also contribute to variations in *in vivo* CA activity; however, these effects are not large (Jenkins *et al.*, 1989). The interaction of β-CA and a CO_2-permeable aquaporin in *Arabidopsis thaliana* has indicated that CA can be localized near the plasma membrane rather than dispersed throughout the mesophyll cytosol (Wang *et al.*, 2016). This may also impact on CA activity and result in another difference between the C_4 species. Other possibilities pertain to differences in anatomical characteristics of leaves. Both CA and PEPC are cytosolic enzymes, and differences in S_m may affect the efficiency with which CA is used. Our results suggest that increasing g_m may be an important way to increase the CO_2 assimilation rate at low intercellular pCO_2, a scenario that may, for example, occur under drought.

Oxygen isotope discrimination and the CO_2 dependence of isotopic equilibrium

As had previously been observed, $\Delta^{18}O$ decreased with reductions in CA activity as CA facilitates the exchange of O_2 between cytosolic water and CO_2 (Fig. 7; Williams *et al.*, 1996; Cousins *et al.*, 2006). Previous reports, which have estimated the proportion of cytosolic CO_2 in equilibrium with leaf water (θ) in C_4 species, have generally assumed a relatively large g_m value and this then led to lower estimates of θ (Cousins *et al.*, 2006, 2008). Here we assumed that in the *S. viridis* null plants there is sufficient CA for isotopic equilibrium to be reached, as discussed by Barbour *et al.* (2016). For comparison, we also estimated g_m from anatomical estimates of S_m, and cell wall and cytosolic thickness following calculations outlined by von Caemmerer and Evans (2015). This gives a g_m value of 0.68 mol m^{-2} s^{-1} bar^{-1} which is less than the value of 0.9 mol m^{-2} s^{-1} bar^{-1} calculated from $\Delta^{18}O$ measurements and highlights the anatomical constraints for CO_2 diffusion dictated by the photosynthetic pathway in leaves of C_4 plants (von Caemmerer *et al.*, 2007).

Reduction in CA activity led to significant reductions in θ but it is interesting to note that θ did not vary significantly with pCO_2. This is explained by the fact that CA activity increases linearly with pCO_2 so that although there is more CO_2 that needs to equilibrate with leaf water, there is also proportionally more CA activity. The fact that neither transgenic line showed a CO_2 dependence suggests that the decrease in the ratio of CA hydrations to PEP carboxylations is not affecting the isotopic equilibration of CO_2 with leaf water. These results have important implications for the interpretation of the ^{18}O signature of atmospheric CO_2 (Yakir and Sternberg, 2000; Gillon and Yakir, 2001; Wingate *et al.*, 2009).

Reduction of CA in S. viridis *does not alter the stomatal reponse to CO_2*

The CO_2 regulation of stomatal conductance remains an open question (Engineer *et al.*, 2016). It has been previously shown that in the *ca1*/*ca4* double mutant of *A. thaliana*, the degree of stomatal closure in response to increasing pCO_2 was reduced (Hu *et al.*, 2010; Wang *et al.*, 2016). It is clear that CA is part of a complex signal transduction network. However, nothing is currently known about the role of CA in stomatal CO_2 responses in C_4 species. In our study, where only one β-CA isoform was reduced, we found no change in the response of stomatal conductance to CO_2. The *S. viridis* β-CA reduced here (Si003882m.g) has low sequence identity (<50%) to all of the Arabidopsis β-CAs, but we would predict that multiple reductions in β-CA isoforms would be required to observe a similar stomatal phenotype in *S. viridis*.

Conclusion

Under current atmospheric conditions, CA activity was not rate limiting for C_4 photosynthesis in *S. viridis.* At lower C_i, which may, for example, occur under conditions of drought, our results suggest that g_m may pose a greater limitation than CA activity. However, it is important to investigate the role of CA on C_4 photosynthesis under a range of environmental conditions such as high temperatures which have recently been suggested to deactivate CA activity in *S. viridis* (Boyd *et al.*, 2015). Here we have shown that *S. viridis* is a useful

model monocot C_4 species that lends itself to molecular manipulation of the C_4 photosynthetic pathway.

Supplementary Data

Supplementary data are available at *JXB* online.

Table S1. Primers used in this study

Figure S1. CA hydration rates at mesophyll pCO_2 in the T_1 plants.

Figure S2. Very low sequence identity (~37%) between the four main *S. viridis* β-CAs.

Figure S3. High sequence identity (87%) of Si003882m.g to the *ZmCA2* (GRMZM2G348512).

Figure S4. CO_2 assimilation rate of the TDL experiment.

Figure S5. Standard error of $\delta^{18}O$ in the reference gas of repeated measurements with the TGA200A.

Acknowledgements

We thank Jasper Pengelly for assisting with construct generation, Xueqin Wang for assisting with *S. viridis* transformations, Soumi Bala for help with biochemical assays, gas exchange, and TDL measurements, and Murray Badger for making the MIMS available for measurements of CA activity. We thank Hilary Stuart-Williams for calibrating standard gases and water samples, and Joyce van Eck and Tom Brutnell for helpful discussions regarding *S. viridis* transformations. We thank Joanne Lee and the Centre for Advanced Microscopy at ANU for technical assistance with microscopy. This research was supported by the Bill and Melinda Gates Foundation's funding for the C_4 Rice consortium and by the Australian Research Council Centre of Excellence for Translational Photosynthesis (CE140100015). RES is funded by ARC DECRA (DE130101760).

References

Alonso-Cantabrana H, von Caemmerer S. 2016. Carbon isotope discrimination as a diagnostic tool for C_4 photosynthesis in C_3–C_4 intermediate species. Journal of Experimental Botany **67,** 3109–3121.

Badger MR, Price GD. 1989. Carbonic anhydrase activity associated with the cyanobacterium Synechococcus PCC7942. Plant Physiology **89,** 51–60.

Badger MR, Price GD. 1994. The role of carbonic anhydrase in photosynthesis. Annual Review of Plant Biology **45,** 369–392.

Barbour MM, Evans JR, Simonin KA, von Caemmerer S. 2016. Online CO_2 and H_2O oxygen isotope fractionation allows estimation of mesophyll conductance in C_4 plants, and reveals that mesophyll conductance decreases as leaves age in both C_4 and C_3 plants. New Phytologist **210,** 875–889

Bartlett JG, Alves SC, Smedley M, Snape JW, Harwood WA. 2008. High-throughput Agrobacterium-mediated barley transformation. Plant Methods **4,** 1–12.

Boyd RA, Gandin A, Cousins AB. 2015. Temperature response of C_4 photosynthesis: biochemical analysis of Rubisco, phosphoenolpyruvate carboxylase and carbonic anhydrase in *Setaria viridis*. Plant Physiology **160,** 1850–1861.

Brutnell TP, Wang L, Swartwood K, Goldschmidt A, Jackson D, Zhu X-G, Kellogg E, Van Eck J. 2010. *Setaria viridis*: a model for C_4 photosynthesis. The Plant Cell **22,** 2537–2544.

Cernusak LA, Farquhar GD, Wong SC, Stuart-Williams H. 2004. Measurement and interpretation of the oxygen isotope composition of carbon dioxide respired by leaves in the dark. Plant Physiology **136,** 3350–3363.

Christin P-A, Boxall SF, Gregory R, Edwards EJ, Hartwell J, Osborne CP. 2013. Parallel recruitment of multiple genes into C_4 photosynthesis. Genome Biology and Evolution **5,** 2174–2187.

Christin PA, Osborne CP. 2013. The recurrent assembly of C_4 photosynthesis, an evolutionary tale. Photosynthesis Research **117,** 163–175.

Cousins AB, Badger MR, von Caemmerer S. 2006. A transgenic approach to understanding the influence of carbonic anhydrase on $C^{18}OO$ discrimination during C_4 photosynthesis. Plant Physiology **142,** 662–672.

Cousins AB, Badger MR, von Caemmerer S. 2008. C_4 photosynthetic isotope exchange in NAD-ME-and NADP-ME-type grasses. Journal of Experimental Botany **59,** 1695–1703.

Cousins AB, Baroli I, Badger MR, Ivakov A, Lea P, Leegood RC, von Caemmerer S. 2007. The role of phosph*enol*pyruvate carboxylase during C_4 photosynthetic isotope exchange and stomatal conductance. Plant Physiology **145,** 1–12.

Craig H, Gordon LI. 1965. Deuterium and oxygen 18 variations in the ocean and the marine atmosphere. In: Tongiorgi E, ed. Proceedings of a Conference on stable isotopes in oceanographic studies and paleotemperatures. Pisa, Italy: Consiglio Nazionale delle Ricerche, Laboratorio di Geologia Nucleare, 9–130.

Curtis MD, Grossniklaus U. 2003. A Gateway cloning vector set for high-throughput functional analysis of genes *in planta*. Plant Physiology **133,** 462–469.

Danila F, Quick WP, White RG, Furbank RT, von Caemmerer S. 2016. The metabolite pathway between bundle sheath and mesophyll: quantification of plasmodesmata in leaves of C_3 and C_4 monocots. The Plant Cell **28,** 1461–1471.

Dever LV. 1997. Control of photosynthesis in *Amaranthus edulis* mutants with reduced amounts of PEP carboxylase. Australian Journal of Plant Physiology **24,** 469–476.

Dever LV, Lea PJ, Blackwell RD, Leegood RC. 1992. The isolation of mutants of C_4 photosynthesis. In: Murata N, ed. Research in Photosynthesis, **Vol. 111**. Kluwer Academic Publishers, 891–894.

DiMario RJ, Quebedeaux JC, Longstreth D, Dassanayake M, Hartman MM, Moroney JV. 2016. The cytoplasmic carbonic anhydrases βCA2 and βCA4 are required for optimal plant growth at low CO_2. Plant Physiology **171,** 280–293.

Doust AN, Kellogg EA, Devos KM, Bennetzen JL. 2009. Foxtail millet: a sequence-driven grass model system. Plant Physiology **149,** 137–141.

Engineer CB, Hashimoto-Sugimoto M, Negi J, Israelsson-Nordstrom M, Azoulay-Shemer T, Rappel WJ, Iba K, Schroeder JI. 2016. CO_2 sensing and CO_2 regulation of stomatal conductance: advances and open questions. Trends in Plant Science **21,** 16–30.

Evans J, Sharkey T, Berry J, Farquhar G. 1986. Carbon isotope discrimination measured concurrently with gas exchange to investigate CO_2 diffusion in leaves of higher plants. Functional Plant Biology **13,** 281–292.

Evans JR, Caemmerer S, Setchell BA, Hudson GS. 1994. The relationship between CO_2 transfer conductance and leaf anatomy in transgenic tobacco with a reduced content of Rubisco. Functional Plant Biology **21,** 475–495.

Evans JR, von Caemmerer S. 1996. Carbon dioxide diffusion inside leaves. Plant Physiology **110,** 339–346.

Farquhar GD, Cernusak LA. 2012. Ternary effects on the gas exchange of isotopologues of carbon dioxide. Plant, Cell and Environment **35,** 1221–1231.

Farquhar G, Lloyd J. 1993. Carbon and oxygen isotope effects in the exchange of carbon dioxide between terrestrial plants and the atmosphere. In: Elheringer JR, Hall AE, Farquhar G, eds. Stable isotopes and plant carbon–water relations. New York: Academic Press, 47–70.

Flexas J, Diaz-Espejo A, GalmES J, Kaldenhoff R, Medrano H, Ribas-Carbo M. 2007. Rapid variations of mesophyll conductance in response to changes in CO2 concentration around leaves. Plant, Cell and Environment **30,** 1284–1298.

Furbank RT, Chitty JA, Jenkins CLD, Taylor WC, Trevanion SJ, von Caemmerer S, Ashton AR. 1997. Genetic manipulation of key photosynthetic enzymes in the C_4 plant *Flaveria bidentis*. Australian Journal of Plant Physiology **24,** 477–485.

Gibson DG, Young L, Chuang RY, Venter JC, Hutchison CA 3rd, Smith HO. 2009. Enzymatic assembly of DNA molecules up to several hundred kilobases. Nature Methods **6,** 343–345.

Gillon J, Yakir D. 2001. Influence of carbonic anhydrase activity in terrestrial vegetation on the ^{18}O content of atmospheric CO_2. Science **291,** 2584–2587.

Gillon JS, Yakir D. 2000. Naturally low carbonic anhydrase activity in C_4 and C_3 plants limits discrimination against $C^{18}OO$ during photosynthesis. Plant, Cell and Environment **23,** 903–915.

Greenup AG, Sasani S, Oliver SN, Talbot MJ, Dennis ES, Hemming MN, Trevaskis B. 2010. ODDSOC2 is a MADS box floral repressor that is down-regulated by vernalization in temperate cereals. Plant Physiology **153,** 1062–1073.

Gutknecht J, Bisson MA, Tosteson FC. 1977. Diffusion of carbon dioxide through lipid bilayer membranes. Effects of carbonic anhydrase, bicarbonate, and unstirred layers. Journal of General Physiology **69,** 779–794.

Hatch MD. 1987. C_4 photosynthesis: a unique blend of modified biochemistry, anatomy and ultrastructure. Biochimica et Biophysica Acta **895,** 81–106.

Hatch MD, Burnell JN. 1990. Carbonic anhydrase activity in leaves and its role in the first step of C_4 photosynthesis. Plant Physiology **93,** 825–828.

Hu H, Boisson-Dernier A, Israelsson-Nordstrom M, Bohmer M, Xue S, Ries A, Godoski J, Kuhn JM, Schroeder JI. 2010. Carbonic anhydrases are upstream regulators of CO_2-controlled stomatal movements in guard cells. Nature Cell Biology **12,** 87–93.

Jenkins CLD, Furbank RT, Hatch MD. 1989. Mechanism of C_4 photosynthesis: a model describing the inorganic carbon pool in bundle sheath cells. Plant Physiology **91,** 1372–1381.

John CR, Smith-Unna RD, Woodfield H, Covshoff S, Hibberd JM. 2014. Evolutionary convergence of cell-specific gene expression in independent lineages of C_4 grasses. Plant Physiology **165,** 62–75.

Lawrence SD, Novak NG, Slack JM. 2003. Epitope tagging: a monoclonal antibody specific for recombinant fusion proteins in plants. Biotechniques **35,** 488–492.

Li P, Brutnell TP. 2011. *Setaria viridis* and *Setaria italica*, model genetic systems for the Panicoid grasses. Journal of Experimental Botany **62,** 3031–3037.

Livak KJ, Schmittgen TD. 2001. Analysis of relative gene expression data using real-time quantitative PCR and the 2(-Delta Delta C(T)) Method. Methods **25,** 402–408.

Matsuoka M, Furbank RT, Fukayama H, Miyao M. 2001. Molecular engineering of C_4 photosynthesis. Annual Review of Plant Physiology and Plant Molecular Biology **52,** 297–314.

Moroney JV, Bartlett SG, Samuelsson G. 2001. Carbonic anhydrases in plants and algae. Plant, Cell and Environment **24,** 141–153.

Okabe K, Yang S-Y, Tsuzuki M, Miyachi S. 1984. Carbonic anhydrase: its content in spinach leaves and its taxonomic diversity studied with anti-spinach leaf carbonic anhydrase antibody. Plant Science Letters **33,** 145–153.

Pengelly JJL, Sirault XRR, Tazoe Y, Evans JR, Furbank RT, von Caemmerer S. 2010. Growth of the C_4 dicot *Flaveria bidentis*: photosynthetic acclimation to low light through shifts in leaf anatomy and biochemistry. Journal of Experimental Botany **61,** 4109–4122.

Pengelly JJL, Tan J, Furbank RT, von Caemmerer S. 2012. Antisense reduction of NADP-malic enzyme in *Flaveria bidentis* reduces flow of CO_2 through the C_4 cycle. Plant Physiology **160,** 1070–1080.

Sage RF, Sage TL, Kocacinar F. 2012. Photorespiration and the evolution of C4 photosynthesis. Annual Review of Plant Biology **63,** 19–47.

Schindelin J, Arganda-Carreras I, Frise E, *et al*. 2012. Fiji: an open-source platform for biological-image analysis. Nature Methods **9,** 676–682.

Sharwood RE, Sonawane BV, Ghannoum O, Whitney SM. 2016. Improved analysis of C_4 and C_3 photosynthesis via refined in vitro assays of their carbon fixation biochemistry. Journal of Experimental Botany **67,** 3137–3148.

Studer AJ, Gandin A, Kolbe AR, Wang L, Cousins AB, Brutnell TP. 2014. A limited role for carbonic anhydrase in C_4 photosynthesis as revealed by a ca1ca2 double mutant in maize. Plant Physiology **165,** 608–617.

Tazoe Y, von Caemmerer S, Estavillo GM, Evans JR. 2011. Using tunable diode laser spectroscopy to measure carbon isotope discrimination and mesophyll conductance to CO_2 diffusion dynamically at different CO_2 concentrations. Plant, Cell and Environment **34,** 580–591.

Vandesompele J, De Preter K, Pattyn F, Poppe B, Van Roy N, De Paepe A, Speleman F. 2002. Accurate normalization of real-time quantitative RT–PCR data by geometric averaging of multiple internal control genes. Genome Biology **3**, Research0034.

von Caemmerer S. 2000. Biochemical models of leaf photosynthesis. Collingwood, Australia: CSIRO Publishing.

von Caemmerer S, Evans JR. 2015. Temperature responses of mesophyll conductance differ greatly between species. Plant, Cell and Environment **38,** 629–637.

von Caemmerer S, Evans JR, Cousins AB, Badger MR, Furbank RT. 2007. C_4 photosynthesis and CO_2 diffusion. In: Sheehy JE, Mitchell PL, Hardy B, eds. Charting new pathways to C_4 rice. Philippines: IRRI, 95–115.

von Caemmerer S, Furbank RT. 2003. The C_4 pathway: an efficient CO_2 pump. Photosynthesis Research **77,** 191–207.

von Caemmerer S, Quinn V, Hancock N, Price G, Furbank R, Ludwig M. 2004. Carbonic anhydrase and C_4 photosynthesis: a transgenic analysis. Plant, Cell and Environment **27,** 697–703.

Wang C, Hu H, Qin X, Zeise B, Xu D, Rappel W-J, Boron WF, Schroeder JI. 2016. Reconstitution of CO_2 regulation of SLAC1 anion channel and function of CO_2-permeable PIP2;1 aquaporin as CARBONIC ANHYDRASE4 interactor. The Plant Cell **28,** 568–582.

Williams TG, Flanagan LB, Coleman JR. 1996. Photosynthetic gas exchange and discrimination against $^{13}CO_2$ and $C^{18}O^{16}O$ in tobacco plants modified by an antisense construct to have low chloroplastic carbonic anhydrase. Plant Physioogy **112,** 319–326.

Wingate L, Ogee J, Cuntz M, *et al*. 2009. The impact of soil microorganisms on the global budget of delta ^{18}O in atmospheric CO_2. Proceedings of the National Academy of Sciences, USA **106,** 22411–22415.

Yakir D, Sternberg LDL. 2000. The use of stable isotopes to study ecosystem gas exchange. Oecologia **123,** 297–311.